Noise Assessment of RPM-Controlled Multirotor Configurations Under Wind Conditions

Jeongwoo Ko[1], Younghoon Kim[1], Jaeheon Jeong[1] and Soogab Lee[2]

[1]Department of Aerospace Engineering, Seoul National University,
Seoul 08826, Republic of Korea
[2]Department of Aerospace Engineering, Institute of Engineering Research,
Seoul National University, Seoul 08826, Republic of Korea
Corresponding Author: *solee@snu.ac.kr*

Abstract

This study performed a real-time prediction of RPM-controlled multirotor noise using a comprehensive multirotor noise assessment (CONA) framework. The key objectives of this study include the synthesis of frequency-modulated multirotor noise and assessment of flyover and takeoff noise under wind conditions. The CONA framework predicted the rotor tonal and broadband noise for a planned mission profile. Gusty wind conditions were efficiently simulated using a Dryden wind turbulence model. When tracking the mission profile under wind conditions, the multirotor noise was characterized by a non-stationary signal with frequency and amplitude modulations. These characteristics induced variations in the noise impact, such as the psychoacoustic metrics. To clarify the effects of wind conditions, prediction-based psychoacoustic analysis were performed for cross- and plus-type quadrotor configurations. The results revealed that the RPM-controlled mechanisms of each configuration were different, indicating that gusty wind conditions exhibited complicated effects on noise impact owing to its mean flow velocity and directions. Moreover, the high-resolution time-frequency analysis illustrated the modulation characteristics of the non-stationary noise signal. The prediction-based psychoacoustic analysis of multirotor noise revealed that the CONA framework facilitated the perception-based evaluation of multirotor configurations in aerial vehicle designs and operations.

1 Introduction

Currently, research on the commercialization of unmanned aerial vehicles (UAV) and urban air mobility (UAM) is being actively conducted. Novel aerial vehicles are new development in the aviation market, and have attracted increasing attention for broad applications, including drone delivery and as a new transportation system in megacities [1]. To enhance their application in urban environments, aerial vehicles should be developed in connection with air traffic management systems and ground infrastructures, such as the vertiport [2]. Furthermore, to ensure its civilian acceptance, it is essential to strictly certify aerial vehicles and conduct a perception-based evaluation at the design stage; thus, it is essential to consider the safety and noise impact of aerial vehicles [3]. Compared to conventional helicopters, the safety and noise impact of novel aerial vehicles can be improved using electric vertical take-off and landing (eVTOL) configurations that adopt RPM-controlled distributed electric propulsion (DEP) systems [4]. Although DEP systems can reduce the noise impact of single flight events, the importance of low-noise design and operations has attracted increasing attention for the commercial use of aerial vehicles in urban environments as it involves numerous operations [5].

Typically, RPM-controlled mechanisms are applied to DEP systems consisting of multiple small rotors [6]. The RPM variations of DEP systems are mainly induced by the flight control and torque ripple of the electric motor [7]. These unsteady blade motions with variations in their angular velocity result in tonal noise with a higher blade passing frequency (BPF) harmonics and differences in the directivity pattern compared to the tonal noise of steady rotations [8]. In RPM-controlled rotors, the broadband noise is modulated by the interaction of the acoustic and the BPF harmonics [9]. Typically, DEP systems-based eVTOL exhibits a lower rotor tip speed than

conventional helicopters, indicating the importance of broadband noise [5]. Modulated tonal and broadband noise can induce the frequency modulation (FM) and amplitude modulation (AM) of RPM-controlled multirotor noise. In addition, owing to the acoustic interference of each rotor noise, a change in the RPM results in a modulation of the noise signal [10]. This indicates that the noise of RPM-controlled multirotor configurations is a non-stationary signal that exhibits unique acoustic signatures in terms of sound pressure level and psychoacoustic metrics.

Owing to the significant difference in the operating conditions and noise characteristics of UAV and UAM compared to those of existing transportation systems, various studies have investigated the response of humans to UAV and UAM noise. Particularly, the psychoacoustic annoyance (PA) of UAV has been investigated using acoustic measurements [11]. For example, Christian and Cabell [12] employed subjective annoyance rating as a hearing test for UAV recording signals and correlated the ratings with noise metrics. Zwicker [13] presented a PA model that can directly calculate the relative annoyance degrees of different noise samples without hearing tests. Although the applicability of this PA model for UAV and UAM is currently being investigated, psychoacoustic analysis has been performed on the measured noise of quadrotor UAV and contra-rotating propeller using PA models [14, 15].

For novel aerial vehicles currently in the development stage, psychoacoustic analysis should be performed using auralization through a numerical approach. Krishnamurthy et al. [16] conducted a prediction-based auralization of collective pitch-controlled quadrotors, which is a six-passenger NASA's conceptual eVTOL UAM design. Based on the synthesized noise time history, they demonstrated the capability of the perception-based design of UAM. For multirotor configurations, mid- and high-fidelity numerical simulations have been conducted using vortex lattice method [17] and computational fluid dynamics [18, 19]. Although these approaches can identify the wake interaction effects on noise, their high computational cost for the real-time noise prediction of RPM-controlled rotors has limited their application to static RPM conditions. In addition, the maneuvering of aerial vehicles under wind conditions is one of the challenges of performing real-time RPM-controlled operation simulations [20]. It is essential to consider the change in noise sources by RPM control under realistic atmospheric conditions.

Particularly, it is difficult to understand the aeroacoustic characteristics of novel aerial vehicles currently under development using experimental approaches. For perception-based evaluations of designs and operations, the noise assessment of UAM maneuvering can be performed using comprehensive numerical framework. Few studies have simultaneously investigated the impact in psychoacoustic metrics and real-time operations under wind conditions. This study aimed to perform the prediction-based psychoacoustic analysis of RPM-controlled multirotor noise under wind conditions. To this end, a prediction-based psychoacoustic analysis of cross- and plus-type quadrotors was conducted to discuss the effects of wind and flight control on psychoacoustic metrics, including the FM and AM characteristics.

2 Methodology

In our previous research [10], a comprehensive multirotor noise assessment (CONA) framework was developed for the real-time noise prediction of RPM-controlled multirotor configurations. Figure 1 shows the process flow of this framework. In this study, broadband noise prediction, phase reconstruction, and psychoacoustics modules were included. The details of other modules can be found in our previous study [10].

2.1 Broadband noise prediction module

This module consisted of a semi-empirical model and Amiet's theory with a wall-pressure spectrum (WPS) model (referred to as the Amiet model in this study). The Brooks, Pope, and Marcolini broadband noise model (BPM model) was used as the semi-empirical model for the prediction of the rotor broadband noise [21]. The BPM model can predict the airfoil self-noise, such as turbulent boundary layer-trailing edge (TBLTE) noise, laminar boundary layer-vortex shedding (LBLVS) noise, and bluntness vortex shedding (BVS) noise. Although the BPM model is a semi-empirical model that is based on the steady flow of a NACA airfoil, it has been widely applied for the prediction of rotor broadband noise using blade element analysis with a quasi-steady assumption [16, 22, 23]. Moreover, TBLTE noise can be calculated using the Amiet model. Amiet's theory is an analytical formulation of TBLTE noise derived from Schwartzschild's solution and Curle's far-field acoustic solutions [24]. This formulation utilizes the wall pressure fluctuations of an airfoil by the turbulent boundary layer, and these fluctuations have been proposed as WPS models by various researchers [25]. For the Amiet's theory, the back-scattering correction formulation [26] and the WPS model propose by Lee and Shum [27] were used. The boundary layer parameters, which were used as inputs for the WPS model, were obtained using XFOIL. Because the Amiet model can only calculate TBLTE noise, LBLVS noise and BVS noise were added using the BPM model.

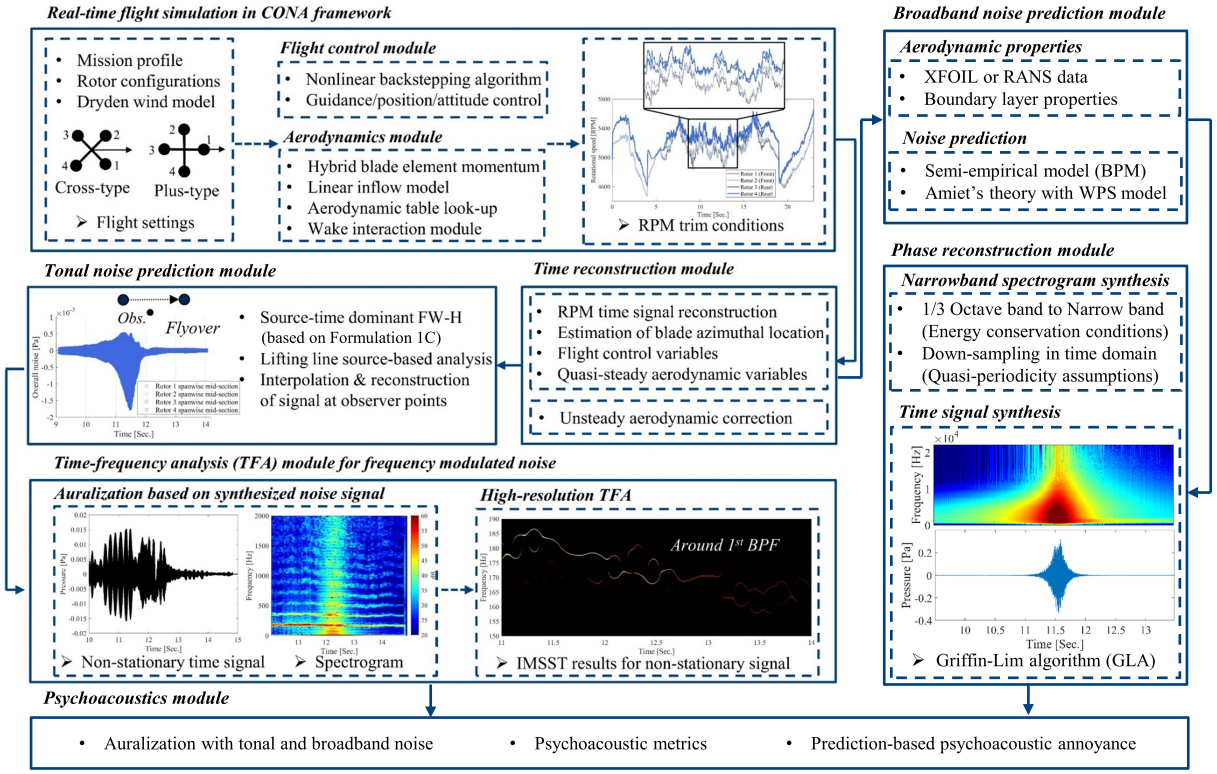

Figure 1: The process flow of CONA framework.

2.2 Phase reconstruction module

An amplitude spectrogram composed of a 1/3 octave band spectrum without phase information was obtained as the output of the broadband noise prediction. For psychoacoustic analyses, broadband noise should be converted to a time signal. Therefore, first, this module performed a narrowband spectrum synthesis (Step I), after which it performed a time signal synthesis through phase reconstruction (Step II). Step I aimed to create a realistic amplitude spectrogram. According to the energy conservation condition, the 1/3 octave band spectrum was converted into a narrowband spectrum. Next, each band was separated based on the user-defined frequency resolution, Δf, and linear interpolation was performed by assigning weight to the noise level based on the adjacent band. Lower bands with smaller bandwidths than Δf were extrapolated to set the lowest frequency of the spectrogram to be the same as Δf. In this study, a narrowband spectrum was constructed using Δf = 25 Hz. Next, down-sampling was performed in the time domain. For each time segment, the window length was set to Δf^{-1}, and the spectrum data included in each segment was averaged; thus, the quasi-periodicity assumption with a uniform window and no-overlap was used. This is because the broadband noise data was derived using the numerical prediction with a quasi-steady assumption. The sampling frequency was set to 44.1 kHz to consider all noise components in the audible frequency range. In Step II, phase reconstruction was performed by applying the Griffin-Lim algorithm (GLA) [28] to the spectrogram created in Step I. The GLA is an iteration-based method for reconstructing phases from an amplitude spectrogram. By randomly initializing the phase spectrogram, GLA utilizes an short-time Fourier Transform (STFT) and inverse STFT iteratively considering the redundancy of the STFT.

2.3 Psychoacoustics module

The psychoacoustic analysis of the time signal of the total noise, which is the sum of the rotor tonal and broadband noise, was performed using a psychoacoustic module. The psychoacoustic metrics considered in this study include loudness, sharpness, fluctuation strength, and roughness. The loudness (N) in sone was calculated using the loudness model proposed by Zwicker (ISO 532-1, [29]), which includes stationary and time-varying metrics. The sharpness (S) in acum was calculated using the standard DIN 45692 [30]. Fluctuation strength (F) in vacil and roughness (R) in asper were calculated using the model proposed by Zwicker and Fastl [13]. These metrics were obtained using the PULSE Reflex software of B&K. The PAs under different flight conditions were compared

using the PA model proposed by Zwicker and Fastl (PA_Z) [13]. This PA model consisted of the 5th percentiles of all time-varying metrics. Although research on whether the existing PA model can be applied to UAVs and UAMs is still in progress, this study proposed a framework for prediction-based PA analysis using this model. This framework can be utilized if an improved model for novel aerial vehicles is developed.

3 Verification and Validation

This study verified and validated broadband noise prediction and psychoacoustics modules. First, the prediction results of the BPM model and Amiet model for the single rotor were compared. Next, the wake interaction effects were illustrated by validating the multirotor configurations, and the limitations of the BPM model were discussed. Lastly, the possibility of extending the BPM model for a prediction-based psychoacoustic analysis using time-signal synthesis procedures was demonstrated. The details of the properties of the validation scenarios can be found in each reference.

3.1 Single rotor hovering flight: Noise spectrum and directivity

The accuracy of the broadband prediction module was confirmed using code verification, and the availability of the BPM and Amiet models were verified by comparing them with another model. An APC 11×4.7 Slow Flyer (SF) rotor with a rotor radius of 0.14 m was used to validate the BPM model and verify the Amiet model [22, 31]. The hovering flight experiment was performed at 3600 RPM, and the microphone was placed at 45° below the rotor disk plane at a distance of 1.905 m from the rotor hub. The results revealed that the Amiet model accurately predicted the noise spectrum, and the BPM model exhibited an error range of ± 3 dB in the mid-frequency range (Fig. 2a). In addition, the low-frequency band and high-frequency band of both models exhibited a significant error because the turbulent ingestion noise (TIN) caused by recirculation and BVS noise, respectively, were not considered. Furthermore, compared to the results of the reference model, the Amiet model exhibited enhanced results, which could be attributed to the fact that the LBLVS noise and back-scattering correction were considered.

A simple rotor in an ideally twisted angle with a section airfoil NACA 0012 was used to validate the Amiet model and verify the BPM model [23]. The rotor was driven at 5465 RPM, and the microphone was located at 35° below the rotor disk plane at a distance of 2.27 m from the rotor hub. The BPM model was fully verified, whereas the Amiet models exhibited an underestimation error of approximately 2–7 kHz (Fig. 2b). Although the BPM model exhibited lower resolutions than the Amiet model under certain conditions, it was suitable for real-time noise prediction owing to its low numerical cost in the design process. In contrast, the Amiet model required a higher numerical cost than the BPM model as it predicts a narrowband spectrum with the predicted boundary layer properties. Therefore, in this study, the BPM model was validated using a more in-depth analysis, and this model was used for the psychoacoustic analysis.

An APC 11×4.7 SF rotor was used to validate the ability of the model to predict noise directivity. The noise directivity patterns of the broadband noise (1–16 kHz) in hovering flight at 2000, 4000, and 6000 RPM were obtained [32]. Microphone arrays were placed at a distance of 1.62 m from the rotor center every 10° from -60° to 60° (0° is rotor disk plane). The model exhibited an error of approximately 3 dB in all cases (Fig. 2c). These results confirm the ability of the BPM model for predicting the acoustic energy in a single rotor hovering flight.

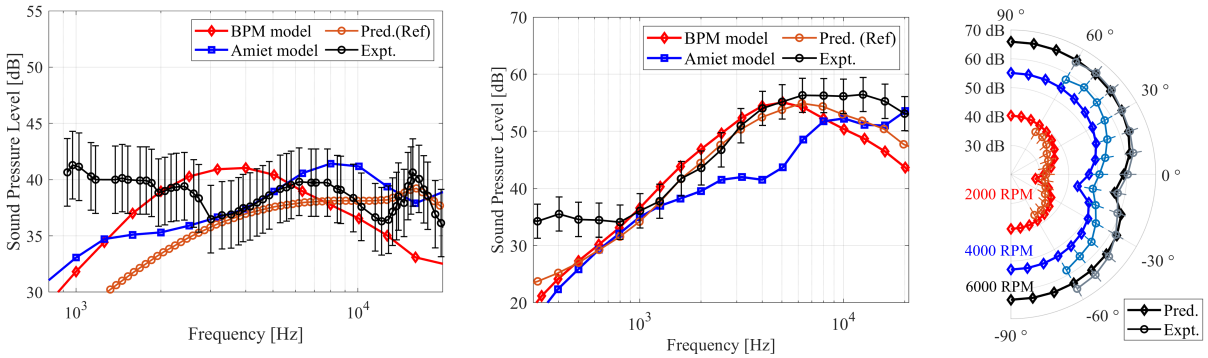

(a) APC 11×4.7 SF rotor

(b) Ideally twisted angle rotor

(c) Noise directivity

Figure 2: Validation results of single rotor hovering flight (Noise spectrum and directivity)

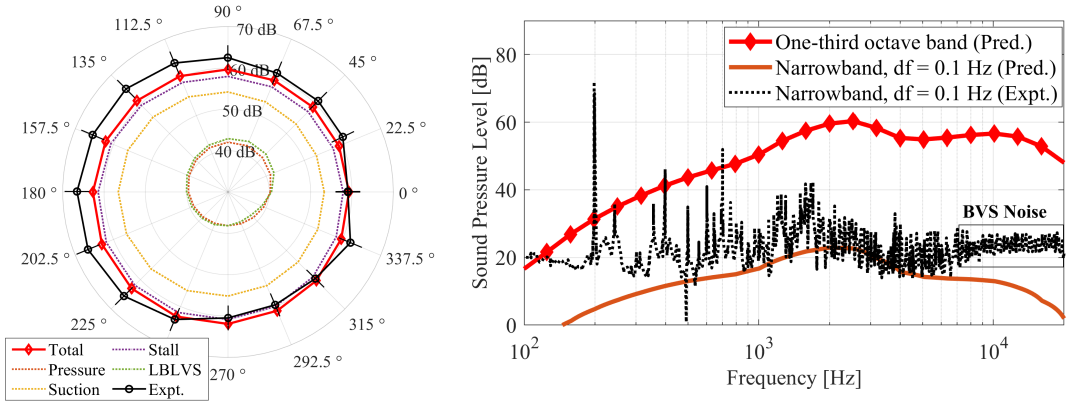

(a) Noise directivity

(b) Noise spectrum at 180°

Figure 3: Validation results of single rotor forward flight (Noise spectrum and directivity)

3.2 Single rotor forward flight: Noise spectrum and directivity

An eHANG Ghost Drone 3.0 blade with a rotor radius of 0.103 m was used to validate the BPM model [33]. The copter pitch angle and flight velocity were set as 15° and 15 m/s, and the circular microphone array was located at a distance of 1.25 m below the center of the rotor disk plane with a diameter of 1.5 m. Microphones were arranged in a counterclockwise direction at intervals of 22.5° by defining 0° as the downstream direction in the wind tunnel. In a forward flight at 6000 RPM, noise directivity patterns were obtained by summation above 6 kHz, and the noise spectrum was measured at 180°. Because the measured noise spectrum was obtained using Δf = 0.1 Hz, the 1/3 octave band results of the BPM model were converted into a narrowband spectrum using the corresponding Δf. In the BPM model, TIN and BVS noise were neglected because there was no information on the wind tunnel turbulence and the geometric properties of the trailing edge, respectively. The prediction errors were less than 3 dB in all angular locations, confirming the high accuracy of the BPM model for predicting radiated noise energy in a single rotor forward flight (Fig. 3a). In addition, the BPM model exhibited reasonable predictions in the mid-frequency range, except at frequency ranges below 1 kHz and above 10 kHz (Fig. 3b). The inability to reasonably predict noise in the low-frequency range could be attributed to the effect of TIN and wind tunnel noise. The prediction in the high-frequency range can be enhanced by adding BVS noise.

3.3 Quadrotor: Noise spectrum and psychoacoustic metrics

This section discusses the validation of the noise spectrum in a quadrotor forward flight and the psychoacoustic metrics in a quadrotor hovering flight. The quadrotor forward flight study discusses the effects of wake interaction on broadband noise and the limitations of the BPM model. The CONA framework considered wake interactions using the parameterized Beddoes wake model [34] (a validated free-wake vortex lattice method solver tuned wake parameters [17]). The details of the method used to adjust wake parameters are described in Ref. [10]. An SUI Endurance cross-type quadrotor was used as the validation model, where R1 and R2 are the front rotors and R3 and R4 are the rear rotors [35]. The experiment was performed at a target vehicle thrust of $45N$, and rotational speed of the R1, R2, R3, and R4 rotors were 4047, 3992, 4895, and 4937 RPM, respectively. In addition, a lateral distance of 3.54 m was fixed between the microphone arrays and the center of the copter, and microphone data was used at a polar angle of 70° (upstream direction is 0°). The noise spectrum in the 1/3 octave band was compared to the prediction results under two scenarios, where one drives R1 and R3 individually (R1 + R3) and the other drives R1 and R3 simultaneously (R1 & R3) to include the wake interaction effect. Figure 4a shows the validation results of both scenarios. In the case of (R1 + R3), the error range was within 3 dB in the frequency range from 0.3–7 kHz, and the prediction in the high-frequency range could be improved by adding BVS noise. In the low-frequency range, TIN, such as recirculation or wind tunnel effects, was dominant. Moreover, the tonal noise related to the rotor–fuselage interaction resulted in low-frequency peaks. In contrast, in the case of (R1 & R3), the BPM model under-predicted the wake interaction effects in all frequency ranges, indicating that the BPM model has limitations in predicting the effects of wake interaction on broadband noise. Although the Beddoes wake model reflected the induced velocity as wake modeling, it was difficult to consider the blade wake interaction (BWI) noise or TIN caused by the wake of the front rotor.

A DJI F450 quadrotor adjusted to 2.0 kg by additional 0.5 kg weights was used as the validation model for the

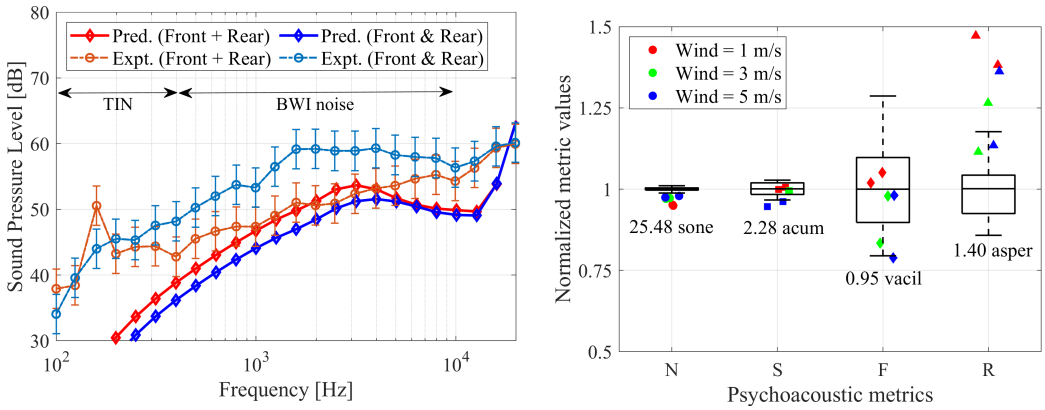

(a) Noise spectrum (forward flight)

(b) Psychoacoustic metrics (hovering flight)

Figure 4: Validation results of quadrotor cases

psychoacoustic metrics [14]. The quadrotor was controlled to hover at 3 m above the ground. The microphone was placed at a distance of 1.5 m above the ground with a distance of 3 m from a quadrotor at an incidence angle of 30°. Experimental results were derived by constructing 45 signals every 4 s using five measurements. For the numerical sound synthesis, hovering flight simulations were performed using different wind profiles (mean velocity = 1, 3, and 5 m/s) using the Dryden wind turbulence model. Observer points were set at azimuthal locations at 0° and 45° relative to the quadrotor arm. All signals were pre-processed to an A-weighted equivalent sound level (L_{Aeq}), 70 dB(A). It was challenging to completely match measurements and numerical environments; thus, the validation was conducted using stationary metrics normalized by the mean values of the experiments. The metrics except the roughness were consistent with the experimental results (scatter plots are numerical results; Fig 4b). Although noise measurements were conducted when the wind velocity was less than 1 m/s, the roughness of the synthesized signal exhibited more similar results under higher wind velocity conditions. Because uncertainties, such as torque ripple conditions, were not considered in the numerical simulation, noise signal modulations were over-predicted as the wind velocity decreased.

4 Prediction-Based Psychoacoustic Analyses

4.1 Mission profiles and flight control

For the psychoacoustic analyses of the RPM-controlled multirotor, a mission profile, including vertical and straight-and-level flight, was selected (as shown in Fig. 5a). A DJI F450 quadrotor, which was used for the validation study in the Sec. 3.3, was used as the reference model. Both observer positions were selected to synthesize the multirotor noise during cruise flight (Observer A) and vertical takeoff (Observer B). Observer A was located 3 m vertically downward from the flight vehicle at 11.5 s, and the flyover noise was synthesized between 9 to 14 s. Observer B was located at the ground takeoff point, and the noise was synthesized between 0.1 to 4 s. The takeoff procedure included the approach of the sinusoidal velocity profile towards the vertically 4 m upward position. In this study, noise synthesis was performed by changing the mean wind speed (V_w) and cruise velocity (V_c). Figure 5b shows the wind speed profiles obtained using the Dryden wind turbulence model at V_w = -2 m/s (minus sign corresponds to the headwind). In addition, although DJI F450 was a cross-type quadrotor, the difference according to the configurations was confirmed by assuming that it was also a plus-type. Figure 6 shows the different RPM trim conditions in both configurations under the same wind condition in Fig. 5b. The cross- and plus-type quadrotors exhibited different RPM control mechanisms for the tracking mission profiles. During cruise flight, the cross-type quadrotor controlled the copter pitch by varying the RPM of two pairs of front and rear rotors, whereas the plus-type quadrotor implemented trim conditions with the side, front, and rear rotors.

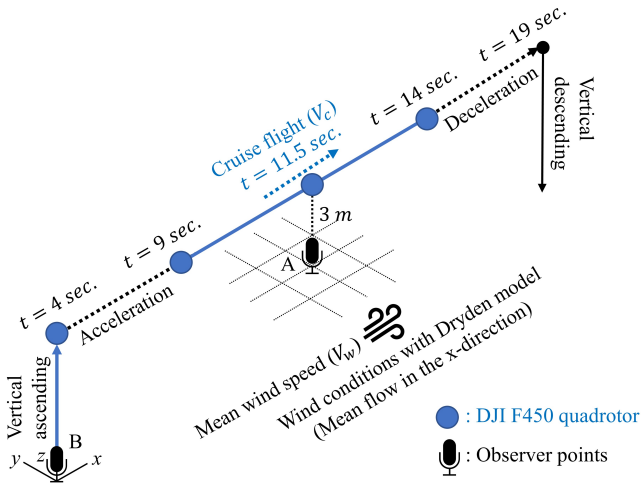

(a) Schematic of mission profile

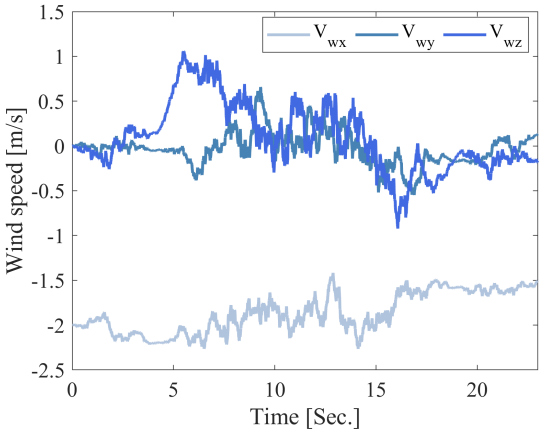

(b) Wind speed at quadrotor (V_w = -2 m/s, headwind)

Figure 5: Mission profile and wind speed profile

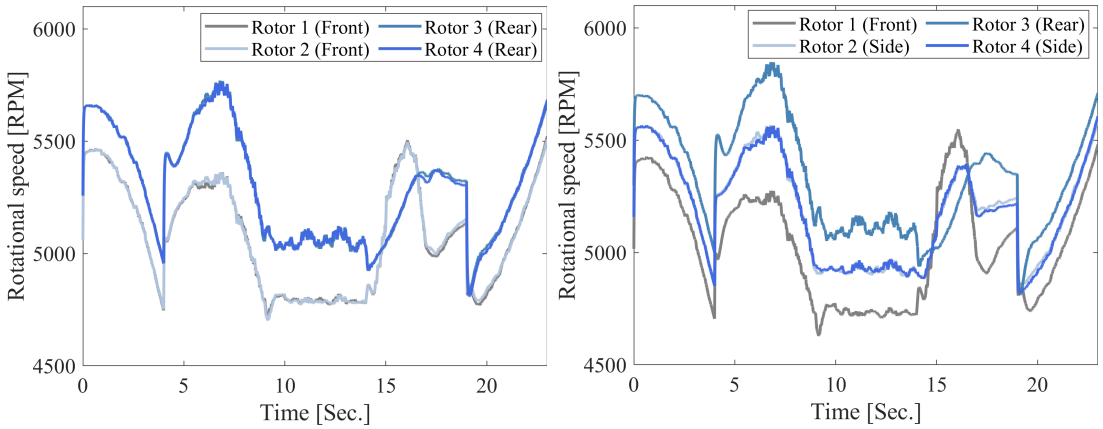

(a) Cross-type quadrotor

(b) Plus-type quadrotor

Figure 6: Time histories of the RPM signal (V_w = -2 m/s, headwind)

4.2 Effects of flight conditions on psychoacoustic annoyance

4.2.1 Observer A: Flyover noise

For the flyover noise, psychoacoustic analyses were performed at V_w = -2 m/s and V_c = 2–10 m/s at an interval of 2 m/s. Normalized psychoacoustic metrics in Fig. 7a were calculated using the 5th percentiles metrics of the cross-type quadrotor at V_c = 2 m/s (N_5 = 15.6 sone; S_5 = 2.28 acum; F_5 = 1.37 vacil; R_5 = 1.825 asper). There was no significant difference in the metrics (except R) with a change in the configurations. Among them, N and S exhibited a linear relationship with V_c. In addition, the N, F, and R metrics tend to increase with an increase in V_c, whereas S tends to decrease with an increase in V_c. Particularly, F increased significantly in the 2–6 m/s range, after which it remained constant with a further increase in the velocity. There was a section where R increased significantly in the cross-type quadrotor at approximately V_c = 6 m/s, which resulted in an increase in PA_Z. The PA_Z of plus-type quadrotor was higher than the that of cross-type quadrotor at lower V_c, and vice-versa at higher V_c (Fig. 7b). This indicated that the acoustic modulation exhibited a significant effect on PA_Z.

Effects of wind speed were confirmed by applying an interval of 1 m/s to V_w = -7–7 m/s when V_c = 10 m/s. Psychoacoustic metrics were normalized based on the 5th percentiles metrics in the wind-off condition of the cross-type quadrotor (N_5 = 20.8 sone; S_5= 1.813 acum; F_5 = 2.309 vacil; R_5 = 2.34 asper). Compared to the effect of V_c, V_w exhibited a more significant non-linear effect on the metrics, which was more pronounced in the cross-type quadrotor (Fig. 8a). In addition, the effect of V_w was almost negligible in F, and in a tailwind, N tends to decrease and S increased. Figure 8b shows that PA_Z decreases in the tailwind for both configurations. Particularly,

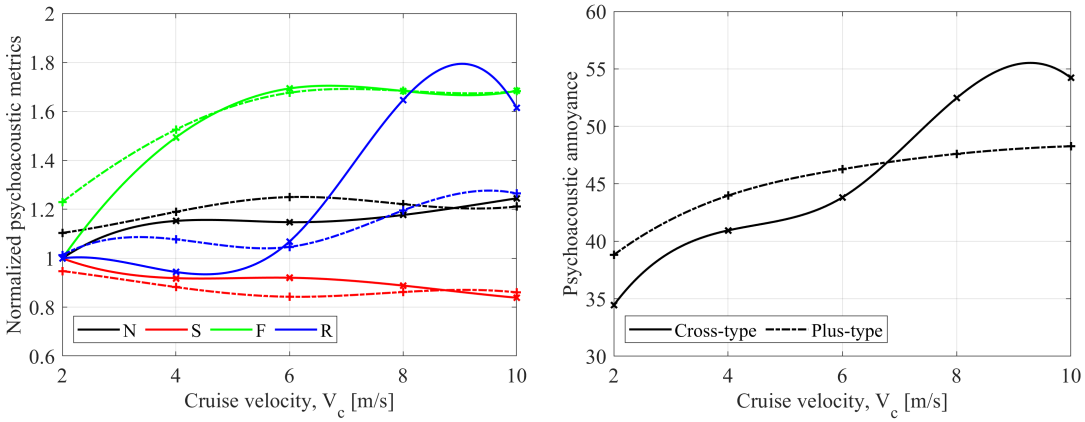

(a) Normalized psychoacoustic metrics

(b) Psychoacoustic annoyance (PA_Z)

Figure 7: Effects of copter velocity on flyover noise (Cross-type: solid line; Plus-type: dashed line)

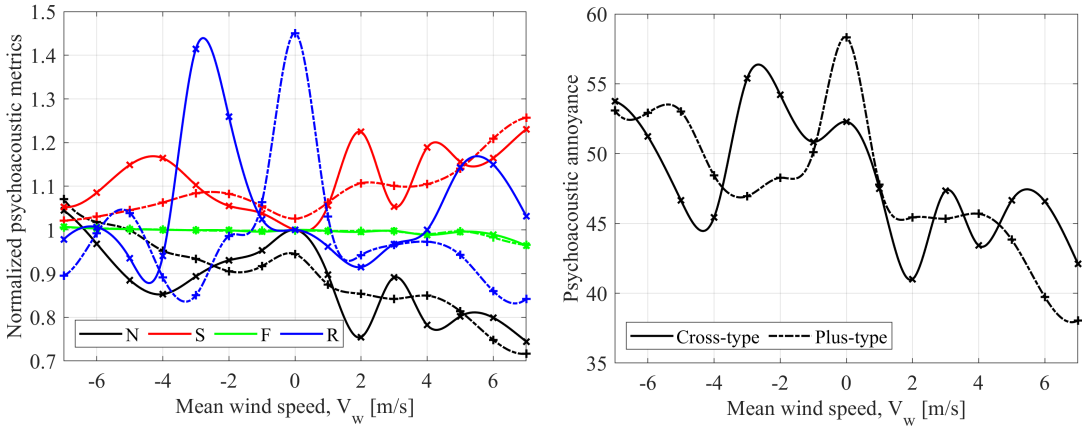

(a) Normalized psychoacoustic metrics

(b) Psychoacoustic annoyance (PA_Z)

Figure 8: Effects of wind speed on flyover noise (Cross-type: solid line; Plus-type: dashed line)

PA_Z reached a peak at the highest R, and this was under the wind-off condition in the plus-type quadrotor. In the wind-off condition, acoustic modulation was only affected by acoustic interference and Doppler effects. In the cross-type quadrotor, constructive and destructive interference occurred more notable because the front and rear rotors were driven at the same RPM; thus, the PA_Z was relatively low in the wind-off condition.

4.2.2 Observer B: Takeoff noise

For the takeoff noise, psychoacoustic analyses were conducted at V_w = 0–7 m/s at an interval of 1 m/s. Psychoacoustic metrics were normalized using the 5th percentiles metrics in the wind-off condition of the cross-type quadrotor (N_5 = 25.17 sone; S_5 = 2.277 acum; F_5 = 2.071 vacil; R_5 = 4.533 asper). Even during takeoff, the RPM control mechanism was different depending on the configurations; thus, the cross- and plus-type quadrotors were compared. As shown in Fig. 9a, compared to those of the cruise flight, the modulation metrics (F and R) tend to decrease with an increase in V_w. In addition, F exhibited a local minimum in the wind-off condition, and the characteristic of the modulation metrics could be attributed to the complicated effects of RPM trim conditions and acoustic interference as a function of the control inputs of takeoff. Figure 9b shows that the PA_Z changes with a change in the modulation metrics, and generally, the PA_Z of the plus-type was higher than that of cross-type. Because takeoff noise was synthesized from the moment of takeoff at the ground, N_5 increased, and PA_Z exhibited a higher value than the flyover noise. These results indicate that the PA in the vertiport is an important factor for noise regulation during actual UAM operation.

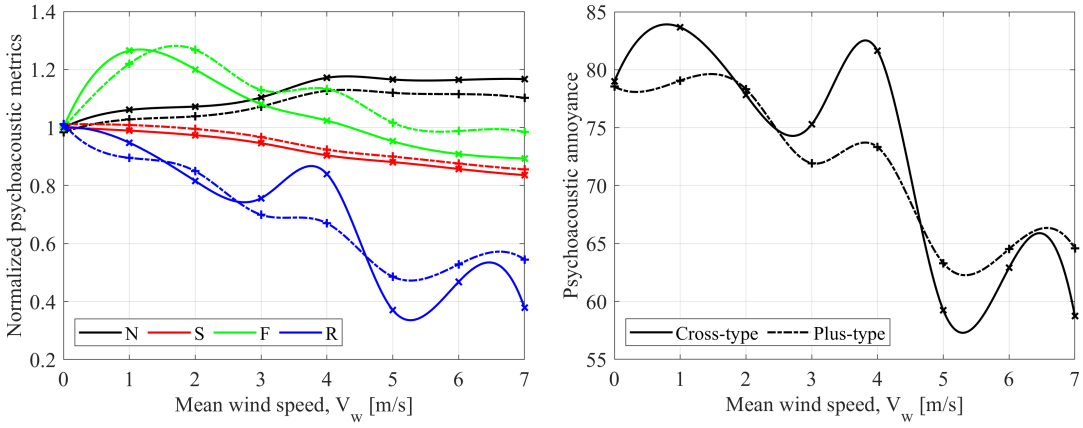

(a) Normalized psychoacoustic metrics

(b) Psychoacoustic annoyance (PA_Z)

Figure 9: Effects of wind speed on takeoff noise (Cross-type: solid line; Plus-type: dashed line)

4.3 High-resolution time-frequency analyses for acoustic modulation

In this section, factors affecting acoustic modulation are discussed using tonal noise. In observer A, effects of configurations were confirmed in the wind-off condition, and in observer B, effects of the wind-on condition were illustrated in the cross-type quadrotor. The non-stationary characteristics of tonal noise induced by the RPM control were demonstrated using the time-frequency analysis (TFA) module of the CONA framework. This module performs high-resolution TFA using the improved multisynchrosqueezing transform (IMSST) [36]. Noise time signal and acoustic modulation around the 1st BPF were illustrated in both observers.

Figure 10 shows the comparison of the flyover noise of the cross- and plus-type quadrotors (V_c = 10 m/s, V_w = 0 m/s). There was no significant difference in the amplitude of the noise time signal, but the AM frequency of the plus-type quadrotor exhibited more complex characteristics. The comparison of the modulation signatures of the 1st BPF noise confirmed that this difference was caused by acoustic interference. For the flyover noise, the Doppler effect resulted in long-period FM along with short-period FM by constructive and destructive interference between the tonal noise of individual rotors. In the cross-type, two pairs of rotors exhibited the same RPM; thus, the modulation frequency was defined as the difference between two RPMs. However, the plus-type quadrotor was operated using three RPMs of the front, rear, and side rotors, so that the modulation frequency consisted of two or more. In the modulation signatures shown in Fig. 10b, acoustic interference occurs alternately in the upper and lower BPF lines. This was one of the causes of the differences in the psychoacoustic metrics with a change in

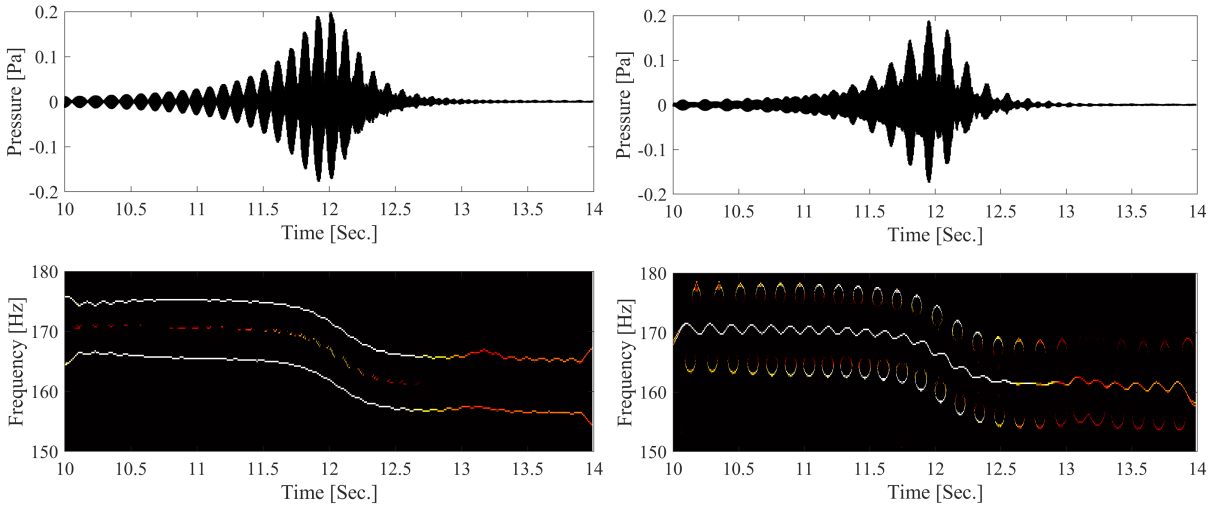

(a) Cross-type (V_c = 10 m/s, V_w = 0 m/s)

(b) plus-type (V_c = 10 m/s, V_w = 0 m/s)

Figure 10: Effects of configurations on acoustic modulation (Noise time signal and IMSST for 1st BPF noise)

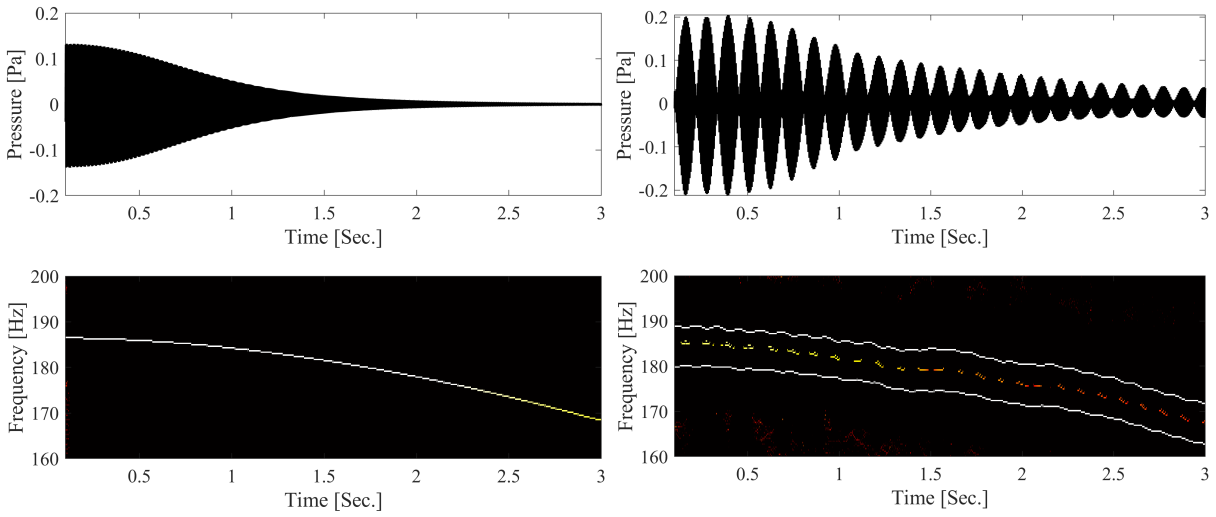

(a) Cross-type (V_w = 0 m/s)

(b) Cross-type (V_w = 3 m/s)

Figure 11: Effects of wind condition on acoustic modulation (Noise time signal and IMSST for 1st BPF noise)

configuration in the flyover noise.

Figure 11 shows the comparison of the takeoff noise in wind-off and wind-on (V_w = 3 m/s) conditions of the cross-type quadrotor. In the noise time signal of the wind-off condition, AM occurred as the distance from observer B to quadrotor increased with a decrease in the RPM of all rotors. However, in the wind-on condition, because the RPM was adjusted for posture control, periodic AM additionally occurred, and the amplitude of the noise time signal was more significant than that in the wind-off condition. This indicates that the wind-on condition is one of the causes of acoustic modulation in the takeoff noise of RPM-controlled DEP system. Observer B was set as the ground takeoff point; thus, the positional relationship with each rotor is the same, and periodic acoustic interference occurred. Because modulation signatures depend on the observer position, it is necessary to examine several representative observers to illustrate the noise impact at the vertiport.

5 Conclusion

In this study, the CONA framework was improved for real-time noise prediction, including rotor tonal and broadband noise. For the perception-based evaluation of multirotor noise, phase reconstruction and psychoacoustics modules were developed to synthesize the time signal of rotor broadband noise and calculate PA, respectively. Based on diverse verification and validation studies, the reliability of the BPM model for UAV rotor noise prediction and psychoacoustic analysis are discussed. The results revealed that the proposed framework can illustrate the effects of configuration, wind speed, and copter velocity on psychoacoustic metrics. The physical and psychoacoustical characteristics of the RPM-controlled multirotor noise were attributed to mission profiles owing to the differences in rotational speed variations, acoustic wave interference, and Doppler shifting. This paper presents fundamental steps toward the prediction-based psychoacoustic analysis of frequency-modulated multirotor noise by developing a comprehensive prediction framework.

Acknowledgments

This work was supported by the National Research Foundation of Korea(NRF) grant funded by the Korea government(MSIT)(No.2021R1A5A1031868). This work was also supported by the KOREA HYDRO & NUCLEAR POWER CO., LTD (No. 2019-Tech-12).

References

[1] S. Rajendran and S. Srinivas, "Air taxi service for urban mobility: a critical review of recent developments, future challenges, and opportunities," *Transportation research part E: logistics and transportation review*, vol. 143, p. 102090, 2020.

[2] A. Straubinger, R. Rothfeld, M. Shamiyeh, K.-D. Büchter, J. Kaiser, and K. O. Plötner, "An overview of current research and developments in urban air mobility–setting the scene for uam introduction," *Journal of Air Transport Management*, vol. 87, p. 101852, 2020.

[3] C. Al Haddad, E. Chaniotakis, A. Straubinger, K. Plötner, and C. Antoniou, "Factors affecting the adoption and use of urban air mobility," *Transportation research part A: policy and practice*, vol. 132, pp. 696–712, 2020.

[4] W. Johnson and C. Silva, "Nasa concept vehicles and the engineering of advanced air mobility aircraft," *The Aeronautical Journal*, vol. 126, no. 1295, pp. 59–91, 2022.

[5] S. A. Rizzi, D. L. Huff, D. D. Boyd, jr., P. Bent, B. S. Henderson, K. A. Pascioni, D. C. Sargent, D. L. Josephson, M. Marsan, H. He, and R. Snider, "Urban air mobility noise: Current practice, gaps, and recommendations," Tech. Rep. TP-2020-5007433, NASA, October 2020.

[6] M. D. Pavel, "Understanding the control characteristics of electric vertical take-off and landing (evtol) aircraft for urban air mobility," *Aerospace Science and Technology*, p. 107143, 2021.

[7] R. McKay and M. J. Kingan, "Multirotor unmanned aerial system propeller noise caused by unsteady blade motion," in *25th AIAA/CEAS Aeroacoustics Conference*, (Delft, The Netherlands), p. 2499, 2019.

[8] J. Jeong, J. Ko, H. Cho, and S. Lee, "Random process-based stochastic analysis of multirotor hovering noise under rotational speed fluctuations," *Physics of Fluids*, vol. 33, no. 12, p. 127107, 2021.

[9] W. J. Baars, L. Bullard, and A. Mohamed, "Quantifying modulation in the acoustic field of a small-scale rotor using bispectral analysis," in *AIAA Scitech 2021 Forum*, (Virtual Event), p. 0713, 2021.

[10] J. Ko, J. Jeong, H. Cho, and S. Lee, "Real-time prediction framework for frequency-modulated multirotor noise," *Physics of Fluids*, vol. 34, no. 2, p. 027103, 2022.

[11] A. J. Torija and C. Clark, "A psychoacoustic approach to building knowledge about human response to noise of unmanned aerial vehicles," *International Journal of Environmental Research and Public Health*, vol. 18, no. 2, p. 682, 2021.

[12] A. W. Christian and R. Cabell, "Initial investigation into the psychoacoustic properties of small unmanned aerial system noise," in *23rd AIAA/CEAS aeroacoustics conference*, p. 4051, 2017.

[13] E. Zwicker and H. Fastl, *Psychoacoustics: Facts and models*, vol. 22. Springer Science & Business Media, 2013.

[14] D. Y. Gwak, D. Han, and S. Lee, "Sound quality factors influencing annoyance from hovering uav," *Journal of Sound and Vibration*, vol. 489, p. 115651, 2020.

[15] A. J. Torija, P. Chaitanya, and Z. Li, "Psychoacoustic analysis of contra-rotating propeller noise for unmanned aerial vehicles," *The Journal of the Acoustical Society of America*, vol. 149, no. 2, pp. 835–846, 2021.

[16] S. Krishnamurthy, S. A. Rizzi, R. Cheng, D. D. Boyd, and A. W. Christian, "Prediction-based auralization of a multirotor urban air mobility vehicle," in *AIAA Scitech 2021 Forum*, (Virtual Event), p. 0587, 2021.

[17] J. Ko, J. Kim, and S. Lee, "Computational study of wake interaction and aeroacoustic characteristics in multirotor configurations," in *INTER-NOISE and NOISE-CON Congress and Conference Proceedings*, vol. 259, pp. 5145–5156, Institute of Noise Control Engineering, 2019.

[18] G. Romani, E. Grande, F. Avallone, D. Ragni, and D. Casalino, "Performance and noise prediction of low-reynolds number propellers using the lattice-boltzmann method," *Aerospace Science and Technology*, p. 107086, 2021.

[19] Z. Jia and S. Lee, "Acoustic analysis of a quadrotor evtol design via high-fidelity simulations," in *25th AIAA/CEAS Aeroacoustics Conference*, (Delft, The Netherlands), p. 2631, 2019.

[20] B. Davoudi, E. Taheri, K. Duraisamy, B. Jayaraman, and I. Kolmanovsky, "Quad-rotor flight simulation in realistic atmospheric conditions," *AIAA Journal*, vol. 58, no. 5, pp. 1992–2004, 2020.

[21] T. F. Brooks, D. S. Pope, and M. A. Marcolini, "Airfoil self-noise and prediction," Tech. Rep. RP-1218, NASA, July 1989.

[22] N. S. Zawodny, D. D. Boyd Jr, and C. L. Burley, "Acoustic characterization and prediction of representative, small-scale rotary-wing unmanned aircraft system components," Tech. Rep. NF1676L-22587, NASA, 2016.

[23] N. A. Pettingill, N. S. Zawodny, C. Thurman, and L. V. Lopes, "Acoustic and performance characteristics of an ideally twisted rotor in hover," in *AIAA Scitech 2021 Forum*, (VIRTUAL EVENT), p. 1928, 2021.

[24] R. K. Amiet, "Noise due to turbulent flow past a trailing edge," *Journal of sound and vibration*, vol. 47, no. 3, pp. 387–393, 1976.

[25] D. Casalino, E. Grande, G. Romani, D. Ragni, and F. Avallone, "Definition of a benchmark for low reynolds number propeller aeroacoustics," *Aerospace Science and Technology*, vol. 113, p. 106707, 2021.

[26] Y. Rozenberg, M. Roger, and S. Moreau, "Rotating blade trailing-edge noise: Experimental validation of analytical model," *AIAA journal*, vol. 48, no. 5, pp. 951–962, 2010.

[27] S. Lee and J. G. Shum, "Prediction of airfoil trailing-edge noise using empirical wall-pressure spectrum models," *AIAA Journal*, vol. 57, no. 3, pp. 888–897, 2019.

[28] D. Griffin and J. Lim, "Signal estimation from modified short-time fourier transform," *IEEE Transactions on acoustics, speech, and signal processing*, vol. 32, no. 2, pp. 236–243, 1984.

[29] *ISO 532-1: 2017(E). Acoustics–methods for calculating loudness–Part 1: Zwicker method.* 2017.

[30] *DIN 45692:2009. Measurement Technique for the Simulation of the Auditory Sensation of Sharpness*. 2009.

[31] S. Li and S. Lee, "Ucd-quietfly: A new program to predict multi-rotor evtol broadband noise," in *Proceedings of the 2020 VFS Aeromechanics for Advanced Vertical Flight Technical Meeting*, (San Jose, California, USA), pp. 21–23, 2020.

[32] R. Gojon, T. Jardin, and H. Parisot-Dupuis, "Experimental investigation of low reynolds number rotor noise," *The Journal of the Acoustical Society of America*, vol. 149, no. 6, pp. 3813–3829, 2021.

[33] H. Hu, Y. Yang, Y. Liu, X. Liu, and Y. Wang, "Aerodynamic and aeroacoustic investigations of multi-copter rotors with leading edge serrations during forward flight," *Aerospace Science and Technology*, vol. 112, p. 106669, 2021.

[34] E. Greenwood II, *Fundamental Rotorcraft Acoustic Modeling from Experiments (FRAME)*. University of Maryland, College Park, 2011.

[35] N. Zawodny and N. Pettingill, "Acoustic wind tunnel measurements of a quadcopter in hover and forward flight conditions," in *INTER-NOISE and NOISE-CON Congress and Conference Proceedings*, vol. 258, pp. 487–500, Institute of Noise Control Engineering, 2018.

[36] G. Yu, "A multisynchrosqueezing-based high-resolution time-frequency analysis tool for the analysis of non-stationary signals," *Journal of Sound and Vibration*, vol. 492, p. 115813, 2021.